Preparation and Mechanical Property of Alumina Fibers Reinforced Thin Architectural Ceramic Plate

Xinzi Zhong
Shaanxi University of Science and Technology
Liyun Cao
Shaanxi University of Science and Technology
J.F. Huang (huangjf@sust.edu.cn)
Shaanxi University of Science and Technology
Yijun Liu
Mona Lisa Group Co., Ltd
Haibo Ouyang
Shaanxi University of Science and Technology
Qinggang Wang
Mona Lisa Group Co., Ltd

Research Article

Keywords: Alumina fibers, Mechanical property, Dispersity, Length-diameter ratio

Posted Date: August 4th, 2021

DOI: https://doi.org/10.21203/rs.3.rs-744889/v1

Abstract

The fibers reinforced thin architectural ceramic plate of 900 mm×1800 mm×2.5 mm with high mechanical property was prepared by a fast-sintering method with a controllable fiber dispersion process. The effects of ball-milling time to the dispersity, average length-diameter ratio and microstructure of alumina fibers were investigated respectively. Meanwhile, the alumina fiber contents to the volume density, water absorption, phase transformation and microstructure of the thin ceramic plate were researched. It is found that the two-steps ball-milling process can control the average length-diameter ratio of the alumina fibers effectively and achieve a well dispersion mixture of fibers and ceramic powders, the fast-sintering method is beneficial for the protection of fiber/matrix interface. The trend of the volume density and bending strength increases with the fiber content from 0 wt% to 5 wt% and then decreases with the fiber content from 5 wt% to 15 wt%. The bending strength of this composite reaches the maximum value of 146.8 MPa with the fiber content is 5 wt%, which is corresponding to the strengthening of alumina fibers and the formation of mullite crystallization in fiber/matrix interface and matrix during the fast-sintering process.

1 Introduction

As a family of architectural ceramic products, the large-sized architectural ceramic plate more than 800 mm×800 mm, is attractive in appearance and convenient for decorating, has attracted research interest. However, the raw materials of the architectural ceramic plate with high energy consumption are non-renewable mineral resources, which is limited and over-exploited [1, 2]. Thus, it is the significant tendency of the architectural ceramic plate to reduce energy consumption, emissions in industrial production and decrease the thickness of the plate to improve the utilization rate of mineral raw materials [3, 4]. In comparison, the thickness of the large-sized thin architectural ceramic plate is only 3 ~ 5 mm, which is 50%~85% thinner on thickness and 40%~53% lower in energy consumption, compared to the architectural ceramic plate with the thickness of 10 ~ 20 mm [5–7]. Unfortunately, the bending strength of the large-sized architectural ceramic plate declines so dramatically with the decrease of thickness that it is unable to mold, corresponding to strong bonding energy of the covalent bond, which has difficulty in slipping, deforming and tending to form brittle fracture in it under external loads [8–10]. Hence, the large-sized thin architectural ceramic plate with the thickness less than 3 mm and enough mechanical property for engineering application is quite difficult to achieve [11].

Various strategies have been proposed to improve the bending strength of the large-sized thin architectural ceramic plate, mainly including increasing the molding pressure and adjusting the composition of ceramic matrix [12, 13], which ultimately improves the bending strength of the large-sized architectural ceramic plate of 900 mm×1800 mm×3 mm to 96 MPa, yet remains to be barely satisfactory in further preparation. Besides, introducing the third phase reinforcement with good creep resistance in ceramic matrix, such as particles and fibers, has proved to be a valid reinforcement method [14]. However, there are still significant challenges to effectively dispersing the fibers in matrix, preventing creep deformation, non-oxide fibers oxidization and controlling the uncontrollable reaction in fiber/matrix

interface over 800℃ to fit production requirements [15, 16]. As a consequence, the above improvements are common in special ceramic and there is too little work has been devoted to the corresponding applications for large-sized thin architectural ceramic plate at present [17, 18].

Inspired by above considerations, to improve the mechanical property of the large-sized thin architectural ceramic plate, we firstly propose a fast-sintering method with the two-steps ball-milling process, which dispersed uniform dispersion of fibers with appropriate aspect ratio into architectural ceramic matrix. And then briefly dispersing optimized inexpensive alumina fibers as reinforcements in matrix and preparing the large-sized thin architectural ceramic plate of 900 mm×1800 mm×2.5 mm. Specially, the bending strength of the reinforced ceramic plate reaches the maximum value of 146.8 MPa with 5 wt% fiber content, corresponding to the strengthening of alumina fibers and the formation of mullite crystallization via fast-sintering method.

2 Experiment

2.1 Preparation of fiber reinforced thin ceramic plate

The preparation process was consisted of the following four steps. First, the optimized alumina fibers (83 wt% θ-Al_2O_3, 12 wt% SiO_2 and 5 wt% Y_2O_3, the average length-diameter ratio is between 80 ~ 85) were immersed in EtOH (C_2H_6O, 99% purity, Sinopharm Chemical Reagent Co., Shanghai, China) via ultrasonic treatment for 40 min.; then the fibers with a certain degree of dispersion were infiltrated in 2.8 mol/L KH570 solution ($C_{10}H_{22}O_4Si$, 95% purity, Sinopharm Chemical Reagent Co., Beijing, China) for surface modification; after that, the mixed solution was stirred gently for 20 min. In the second step, the preliminarily dispersed alumina fibers were weighed based on the mass ratio of 1 wt%, 3 wt%, 5 wt%, 7 wt% and 10 wt% for ceramic powders; then the alumina fibers, EtOH and 0.5 ~ 0.8 mm talumina ballstone were evenly mixed in jar mill with the mass ratio of alumina fibers: ballstone: EtOH = 1:1.5:1; after that, the first-step ball-milling process was carried out for 3 min., 5 min., 7 min., 10 min. and so on. In the third step, the alumina fibers were optimized via optical microscope and vertical centrifuge, then the chopped fibers were evenly mixed up with the ceramic powders whose composition was illustrated in Table 1 via second-step ball-milling method. In the fourth step, the mixture powders were molded to 900 mm×1800 mm×2.5 mm as forming green body under the pressure of 35 MPa, and then the alumina fibers reinforced thin architectural ceramic plate was prepared via fast-sintering at 1200℃ for 30 min.

Table 1
Main chemical composition of ceramic matrix

Chemical composition	Al_2O_3	SiO_2	Fe_2O_3	CaO	MgO	TiO_2	Na_2O	K_2O	IL
Content(wt%)	49.94	37.62	0.41	0.32	0.72	0.38	1.86	2.84	5.91

2.2 Characterization

The microstructure of optimized alumina fibers was observed by high power optical microscope (model EVOS M7000, China) and a vertical centrifuge (model TG-20W, Germany). The scanning electron microscopy (SEM, JSM-IT200, Japan) was used to observe the morphology of dispersed alumina fibers and the cross-section microstructure etched by 1.6 mol·L^{-1} hydrofluoric acid. The phase compositions were characterized by an X-ray diffraction (XRD, Empyrean Alpha-1, Malvern) under the diffraction conditions of Cu and K_{α}. Meanwhile, the diffraction angle parameters were set as 10°~85°, the scanning speed was 5°/min. The bending strength of the samples was characterized by three point bending method in universal mechanical testing machine (CTM2050, China), the average value of five parallel samples reduces the errors of measurement. Moreover, the water absorption of the thin plate must be less than 0.5% according to the ISO 10545-3-2018 [19]. The volume density was measured by the Archimedes method, which could be calculated according to the following formula:

$W=(B-G)/G$ (Eq. 1)

where W represented the value of water absorption, B denoted the mass value after absorbing water and G represented the mass value after drying.

3 Results And Discussion

3.1 Effects of ball-milling time on microstructure and dispersity of fibers

Fig. 1 shows the morphology of dispersed alumina fibers after the first-step ball-milling process in different ball-milling time. Most of the original fibers intertwine together and form cross-linked stable structure (Fig. 1 (a)), which results from electrostatic attraction between fibers. The dispersion of alumina fibers after the first-step ball-milling process for 5 minutes is improved obviously (Fig. 1 (b)), confirming that the short-time friction unties the cross-linked structure and disperses fibers effectively. As deteched in Fig. 1 (c), alumina fibers treated for 10 minutes lose their original fibrous structure, which may attribute to the drastic and long-time physical friction, promoting the cleavage of the inner fiber grains. Fig. 1 (d, e, f) shows the dispersion of alumina fibers in matrix after the second-step ball-milling process in different milling time. It can be found that ceramic powders obviously agglomerated distribute in-homogeneously around dispersed alumina fibers (Fig. 1 (d)), this is because original ceramic powders are too agglomerating to infiltrate evenly into the inner cross-linked space. Ulteriorly, the numerous inter-space between uneven matrix and alumina fibers may lead to weak bonding between fiber/matrix interface, which can't transfer the internal stress from matrix to fibers in time while carrying external loads [20-21]. Besides, the alumina fibers treated for 1 minute in the second-step ball-milling process are uniformly distributed in ceramic powders (Fig. 1 (e)), revealing the two-steps ball-milling process can achieve a well dispersion mixture of fibers and ceramic powders. Inversely, the fibrous structure of fibers is destroyed absolutely over 3 minutes (Fig. 1 (f)), which is consistent with the analysis in Fig. 1 (c).

Fig. 2 (a) shows the average length-diameter ratio of fibers after the first-step ball-milling process in different ball-milling time. The average length-diameter ratio of fibers decreases tardily from 83.8 to 58.9

with the ball-milling time from 0 minutes to 5 minutes, and then declines drastically from 58.9 to 4.6 with the time from 5 minutes to 10 min., illustrating that the friction between fibers and ballstone has a top priority to disperse the cross-linked structure, and then chiefly damages the original fibrous structure of fibers, decreasing the average length-diameter ratio. Notably, the alumina fibers with little average length-diameter ratio by long-time friction are difficult to deflect micro-crack paths effectively, which is adverse to promoting the mechanical property of the thin architectural ceramic plate [22]. In comparison, the average length-diameter ratio of fibers after the second-step ball-milling process decreases sharply from 58.9 to 7.6 with the time from 0 minutes to 3 minutes (Fig. 2 (b)). Besides, the drop rate of it is much faster than that in Fig. 2 (a), which is corresponding to the synergistic drastic friction of matrix, fibers and ballstone. Based on above results, the first-step ball-milling for 5 minutes followed by the second-step ball-milling for 1 minute is proved to be the best two-steps ball-milling process.

3.2 Effects of alumina fiber contents on the thin ceramic plate

Fig. 3 shows the optical photos of the as-prepared thin architectural ceramic plate. Meanwhile, the XRD patterns of samples with different alumina fibers contents are shown in Fig. 4, it is observed that the diffraction peaks of 25.7°, 35.2°, 38.1°, 43.5°, 52.6° and 57.9° agree well with the α-Al_2O_3 (PDF no. 50-0741), illustrating the main crystal phase of fibers transforms from θ-Al_2O_3 to α-Al_2O_3 by fast-sintering method [23]. In comparison, the alumina fibers of α-Al_2O_3 have higher tensile strength than the fibers of θ-Al_2O_3, further confirming that the fast-sintering method with short holding time is beneficial to promoting the mechanical properties of alumina fibers as the reinforcement instead of damaging them unilaterally. Besides, the diffraction peaks of 16.4°, 26.3°, 33.3°, 40.8° and 60.9° can be indexed to the mullite (PDF no. 15-0776), attributing to the appropriate phase ratio of alumina and silicon in glass phase. Furthermore, the mass ratio of alumina to silicon of the fibers is 7.85 which is much higher than that of the matrix of 1.51, the fused alumina phase in fibers may infiltrate into the glass phase in fast-sintering process, which collectively increases the alumina content in liquated glass phase and promotes the crystallization of mullite and whiskers [24,25].

Fig. 5 shows the cross-section SEM images of the as-prepared samples with different alumina fiber contents. It can be noticed that the particles without obvious coarse grains of the cross-section sintered at 1200℃ for 30 minutes is compact (Fig. 5 (a)), suggesting that the fast-sintering system is suitable. Meanwhile, the alumina fibers are perpendicular to the cross-section and embed tightly in the matrix (Fig. 5 (b)), this is because fibers and surrounding matrix are subjected to tensile and compressive stress respectively during the fast-sintering process, which results from thermal expansion coefficient difference between alumina fiber of 9.2×10^{-6}/℃ and matrix of 4.8×10^{-6}/℃ [26]. Namely, the existence of internal stress is beneficial to offset the external stress loads and improve the bending strength of the thin architectural ceramic plate. However, it is the matrix that mainly bears the loads at this moment limited by only 3 wt% fibers contents. As shown in Fig. 5 (c, d), the number of pores in matrix increases obviously with the fiber content more than 5 wt% and fibers in the cross-section of the thin ceramic plate disperse

uniformly. Close observation reveals that there are numerous white substances in the pores of the matrix, which is presumed to be the in-situ fibrous mullite and whiskers conformed by the analysis in Fig. 4.

Fig. 6 shows the volume density and water absorption of the thin architectural ceramic plate with different alumina fiber contents. On the one hand, the volume density of the thin plate increases slowly from 2.722 $g \cdot cm^{-3}$ to 2.733 $g \cdot cm^{-3}$ with the fiber content from 0 wt% to 5 wt%, which mainly ascribes to the density of alumina fibers for 6.22 $g \cdot cm^{-3}$ is much higher than that of matrix for 2.722 $g \cdot cm^{-3}$. On the other hand, the volume density of the thin plate decreases from 2.782 $g \cdot cm^{-3}$ to 2.587 $g \cdot cm^{-3}$ with the fiber content from 5 wt% to 15 wt%, attributing to the inner pores increase in matrix. Simultaneously, the water absorption of the thin architectural ceramic plate decreases tardily from 0.172% to 0.152% with the fiber content from 0 wt% to 5 wt%, further confirming that the in-situ mullite and whiskers during the fast-sintering method can fill the inner pores and increase the compactness of ceramic matrix.

Fig. 7 shows the bending strength of the thin architectural ceramic plate with different alumina fiber contents. The bending strength of 0 wt%, 1 wt%, 3 wt%, 5 wt%, 7 wt%, 11 wt% and 15 wt% fiber contents are 86.2 MPa, 93.8 MPa, 122.4 MPa, 146.8 MPa, 136.2 MPa, 80.3 MPa and 51.5 MPa, respectively. Moreover, the maximum bending strength of the thin architectural ceramic plate reaches 146.8 MPa that is 70.31% higher than the blank sample of 86.2 MPa with 5 wt% fiber contents, which is corresponding to the strengthening of alumina fibers and the formation of mullite crystallization of the matrix during the fast-sintering process.

3.3 Microstructure analysis

Fig. 8 shows the cross-section SEM images of the as-prepared samples with 5 wt% alumina fiber content. Apparently in Fig. 8 (a, b), the expanding micro-cracks which are supposed to be single orientation are deflected to be discontinuous or winding orientation by inner particles and fibers, indicating that the reinforcements can slow down the prolongation speed of micro-cracks in matrix and retard the stress concentration in the micro-crack tip owing to the Griffith micro-crack theory [27,28]. Combined with the EDS analysis of spot 1 with the mass contents of Al, Si, O and Y are 36.95 wt%, 8.5 wt%, 41.02 wt% and 9.26 wt% (Fig. 8 (e)), illustrating that there are alumina fibers embed tightly in the matrix. In addition, the fiber/matrix interface has clear boundaries after the fast-sintering method and there is plenty of white substance in it, suggesting that the fast-sintering method is appropriate and it can prevent the fiber/matrix interface from excessive thermodynamics damage. To clarify the components of the white substance in fiber/matrix interface, the EDS analysis of spot 2 is analyzed in Fig. 8 (f), proving that it is the mullite with the mass contents of Al, Si and O are 41.22 wt%, 11.45 wt% and 42.86 wt%, severally. Fig. 8 (b, c and d) shows the distribution of reinforcements along the fracture micro-cracks. It is found that there are not only thick fibers but also finer fibrous substance at the micro-cracks fracture, both of them are bridge-pulled out of the matrix. Ulteriorly, as shown in Fig. 8 (g, h), the element mass contents of the thick fiber at spot 3 are 32.47 wt% Al, 10.58 wt% Si, 39.68 wt% O, 11.21 wt% Y and the finer fiber at spot 4 are 38.32 wt% Al, 14.18 wt% Si and 45.17 wt% O, respectively. It can be accurately inferred that the thick fiber is alumina fiber and the finer fiber is fibrous mullite that is precipitated out by crystallization in

matrix. Hence, the reinforcements of alumina fibers, particles and in-situ fibrous mullite in matrix and fiber/matrix interface are beneficial to deflecting the paths of the micro-cracks (Fig. 9), which can synergistically slow down the prolongation speed of inner micro-cracks and enhance the mechanical property of the large-sized thin architectural ceramic plate.

4 Conclusion

In summary, the alumina fibers reinforced thin architectural ceramic plate of 900 mm×1800 mm×2.5 mm with high mechanical property is successfully prepared by the fast-sintering method with a controllable fiber dispersion method. It is found that the first-step ball-milling for 5 minutes followed by the second-step ball-milling for 1 minute is proved to be the best two-steps ball-milling process, which can evenly disperse fibers with an appropriate average length-diameter ratio in matrix. The fast-sintering method can prevent the fiber/matrix interface from excessive thermodynamics damage and promote the fast crystallization process of mullite, which is beneficial to improve the mechanical property of this thin plate. The maximum bending strength of the thin plate with 5 wt% alumina fibers contents is 146.8 MPa that is 70.31% higher than the blank sample of 86.2 MPa, corresponding to the strengthening of alumina fibers and the formation of mullite crystallization in fiber/matrix interface and ceramic matrix. In addition, the micro-cracks deflection, particle diffusion enhancement and fiber bridge-pull out of the matrix by particles, alumina fibers and in-situ fibrous mullite, are proved to be the main reinforcement mechanisms. We expect that our findings will have a guiding significance for industrial production and future research of the large-sized thin architectural ceramic plate.

Declarations

Acknowledgements

Authors thank to Shaanxi Key Laboratory of Green Preparation and Functionalization for Inorganic Materials for their experimental platform and testing conditions. This work was supported by the National Natural Science Foundation of China (No. 52073166), the Xi’an Key Laboratory of Green Manufacture of Ceramic Materials Foundation (No. 2019220214SYS017CG039), the Key Program for International S&T Cooperation Projects of Shaanxi Province (2020KW-038, 2020GHJD-04), Science and Technology Program of Xi'an, China (2020KJRC0009) and Scientific Research Program Funded by Shaanxi Provincial Education Department (No. 20JY001), Science and Technology Resource Sharing Platform of Shaanxi Province (2020PT-022), Science and Technology Plan of Weiyang District, Xi'an (202009).

References

1. Renato SM, Almeida H, Farhandi K, Tushtev K, Rezwan, Joining oxide ceramic matrix composites by ionotropic gelation, International Journal of Applied Ceramic Technology, 2020, 17 (4)
2. Singh Abhendra K, Kaitlyn J, Hannah H, Allison V, Daniel B, Zach, Environmental effects on the strength and impact damage resistance of alumina based oxide/oxide ceramic matrix composites,

Ceramics International, 2021, 47 (12)

3. Belfiore Cristina M, Amato Chiara P, Antonino V, Marco, An end of waste alternative for volcanic ash: a resource in the manufacture of ceramic tiles, Construction and Building Materials, 2020, 263
4. Venturelli M, Brough D, Milani M, Montorsi L, Comprehensive numerical model for the analysis of potential heat recovery solutions in a ceramic industry, International Journal of Thermofluids, 2021, 10
5. Xue ZN, Tian XG, Luan TL, Liu JL (2021) Size effect on heat conduction and associate thermal fracture behavior of thin ceramic plates. Theoretical and Applied Fracture Mechanics, p 113
6. Yoshinori Itaya H, Hanai N, Kobayashi T, Nakagawa, Drying-induced strain-stress and deformation of thin ceramic plate, ChemEngineering, 2020, 4 (1)
7. Hiroyuki Miyazaki K, Hirao, Round-robin exercise on the three and four point flexural strength of thin ceramic plates for power modules, International Journal of Applied Ceramic Technology, 2019, 16 (6)
8. Amani Khaskhoussi L, Calabrese J, Bouaziz E, Proverbio, Performances and aging stability of new Al_2O_3-ZrO_2-TiO_2 ternary ceramic composites, Materials Chemistry and Physics, 2020, 243
9. Sadowski T, Marsavina L, Craciun E, Pietras D, Description of brittle behaviour of alumina/zirconia phase ceramics, IOP Conference Series: Materials Science and Engineering, 2018, 416 (1)
10. Simanchal Kar S, Kumar PP, Bandyopadhyay S, Paul, Grinding of hard and brittle ceramic coatings: force analysis, Journal of the European Ceramic Society, 2020, 40 (4)
11. Beatriz Defez GP, Fajarnés I, Tortajada F, Brusola S, Morillas, Flexural strength evaluation of nonconstant thickness ceramic floorings by means of the finite element method, International Journal of Applied Ceramic Technology, 2010, 7 (2)
12. Cui K, Zhang Y, Fu T et al (2020) Toughening mechanism of mullite matrix composites: a Review. Coatings 10(7):672
13. Yang M, Luo X, Yi J et al (2018) A novel way to fabricate fibrous mullite ceramic using sol-gel vacuum impregnation. Ceram Int 44(11):12664–12669
14. Zhang GX, Liu YJ, Lv ZW, Wang J, Zhang WY, Wu Y, Research on impact resistance of ceramic matrix composites, Composite Structures, 2021, 268
15. Chen J, Yang H, Chadeyron R (2014) Tuning the interfacial reaction between CaO-SrO-Al_2O_3-B_2O_3-SiO_2 sealing glass-ceramics and Cr-containing interconnect: crystalline structure vs glass structure. J Eur Ceram Soc 34(8):1989–1996
16. Rizal S, Nakai Y, Shiozawa D et al (2019) Evaluation of interfacial fracture toughness and interfacial shear strength of Typha spp: fiber/polymer composite by double shear test method. Materials 12(14):2225
17. De Villoria RG, Miravete A (2007) Mechanical model to evaluate the effect of the dispersion in nanocomposites. Acta Mater 55(9):3025–3031
18. Fedelinski P (2021) Effective elastic properties of composites with randomly distributed thin rigid fibres. Arch Appl Mech 91(1):135–149

19. ISO 10545-3-2018: Ceramic Tiles Part 3: Determination of water absorption, apparent porosity, apparent relative density and bulk density, 2018
20. Lee JK (2008) A study on validity of using average fiber aspect ratio for mechanical properties of aligned short fiber composites with different fiber aspect ratios. Arch Appl Mech 78(1):1–9
21. Shokrieh MM, Moshrefzadeh-Sani H (2016) An optimized representative volume element to predict the stiffness of aligned short fiber composites. J Compos Mater 50(23):3301–3310
22. Deng Y, Li W, Wang R et al (2016) The temperature-dependent fracture models for fiber-reinforced ceramic matrix composites. Compos Struct 140:534–539
23. Tamura Y, Moshtaghioun BM, Gomez-Garcia D et al (2017) Spark plasma sintering of fine-grained alumina ceramics reinforced with alumina whiskers. Ceram Int 43(1):658–663
24. De Aza AH, Turrillas X, Rodriguez MA et al (2014) Time-resolved powder neutron diffraction study of the phase transformation sequence of kaolinite to mullite. J Eur Ceram Soc 34(5):1409–1421
25. Fernandes RR, van de Werken N et al, Experimental investigation of additively manufactured continuous fiber reinforced composite parts with optimized topology and fiber paths, Additive Manufacturing, 2021: 102056
26. Zubashchenko RV, Formation of composite material fiber-reinforced structure with ceramic aluminosilicate matrix, refractories and industrial ceramics, 2018, 59 (1): 91–94
27. Xu R, Hu XZ, Effects of nanograin structures and surface defects on fracture of microscaled polysilicon components, Journal of the American Ceramic Society, 2020, 103 (6)
28. Lü NC, Cheng YH, Ji JL (2012) Two fracture dynamics problems of fiber reinforced ceramics. Key Eng Mater 18(9):25–34

Figures

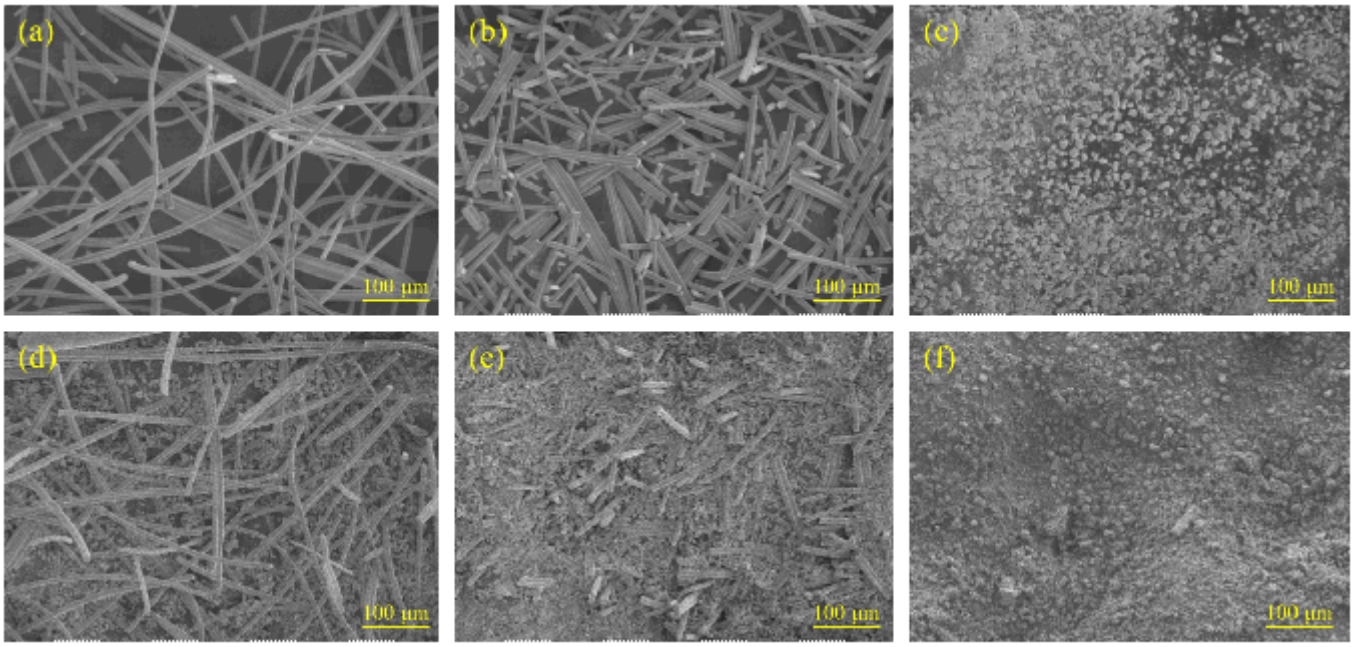

Figure 1

SEM images of the morphology and dispersity of alumina fibers in different ball-milling time; after the first-step ball-milling process (a) 0 min.; (b) 5 min.; (c) 10 min.; and after the second-step ball-milling process (d) 0 min.; (e) 1 min.; (f) 3 min.

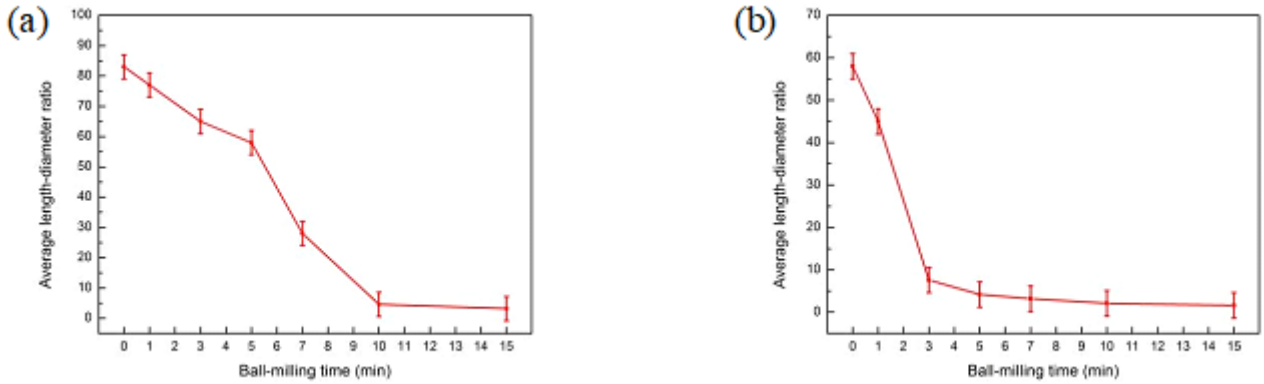

Figure 2

The average length-diameter ratio of alumina fibers in different ball-milling time; (a) the first-step ball-milling process; (b) the second-step ball-milling process.

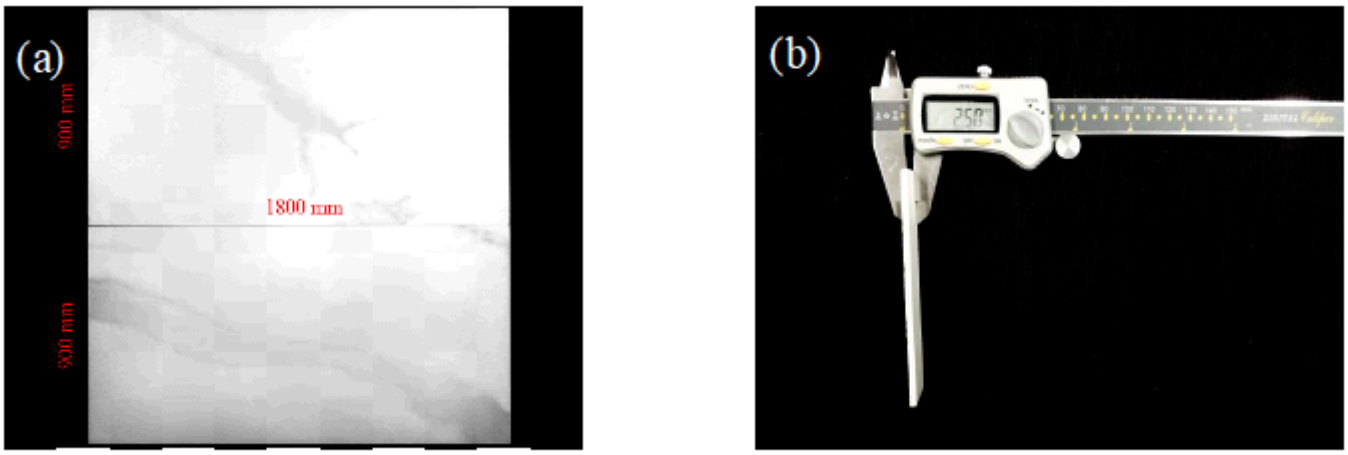

Figure 3

The optical photos of the as-prepared thin architectural ceramic plate; (a) the sample of the prepared product; (b) the sample for characterization.

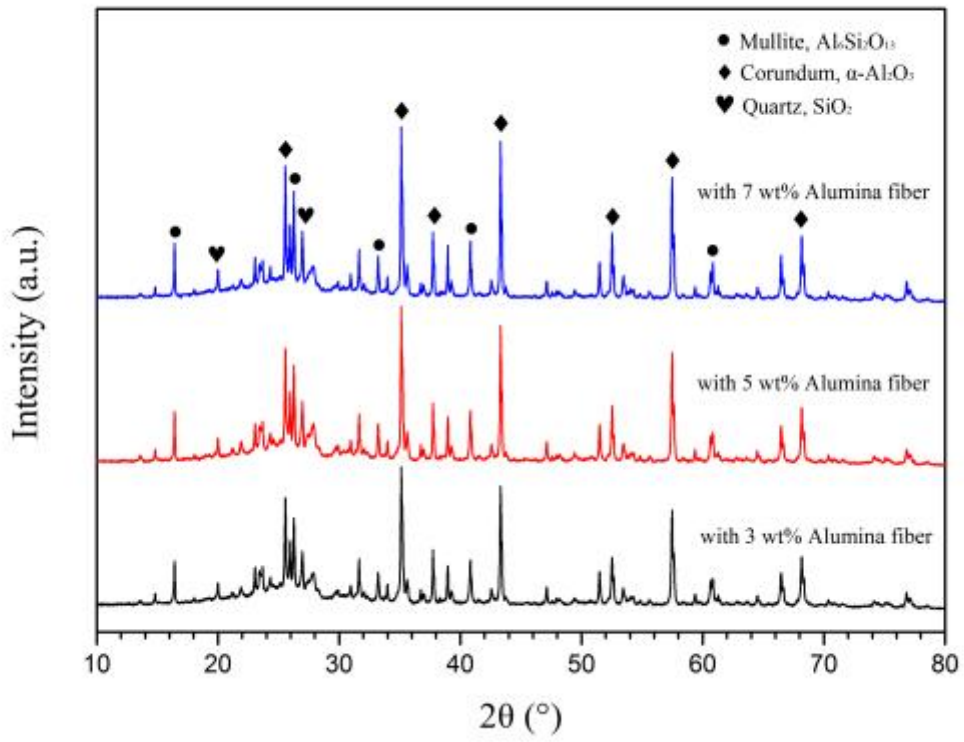

Figure 4

The XRD patterns of the thin architectural ceramic plate with different alumina fiber contents.

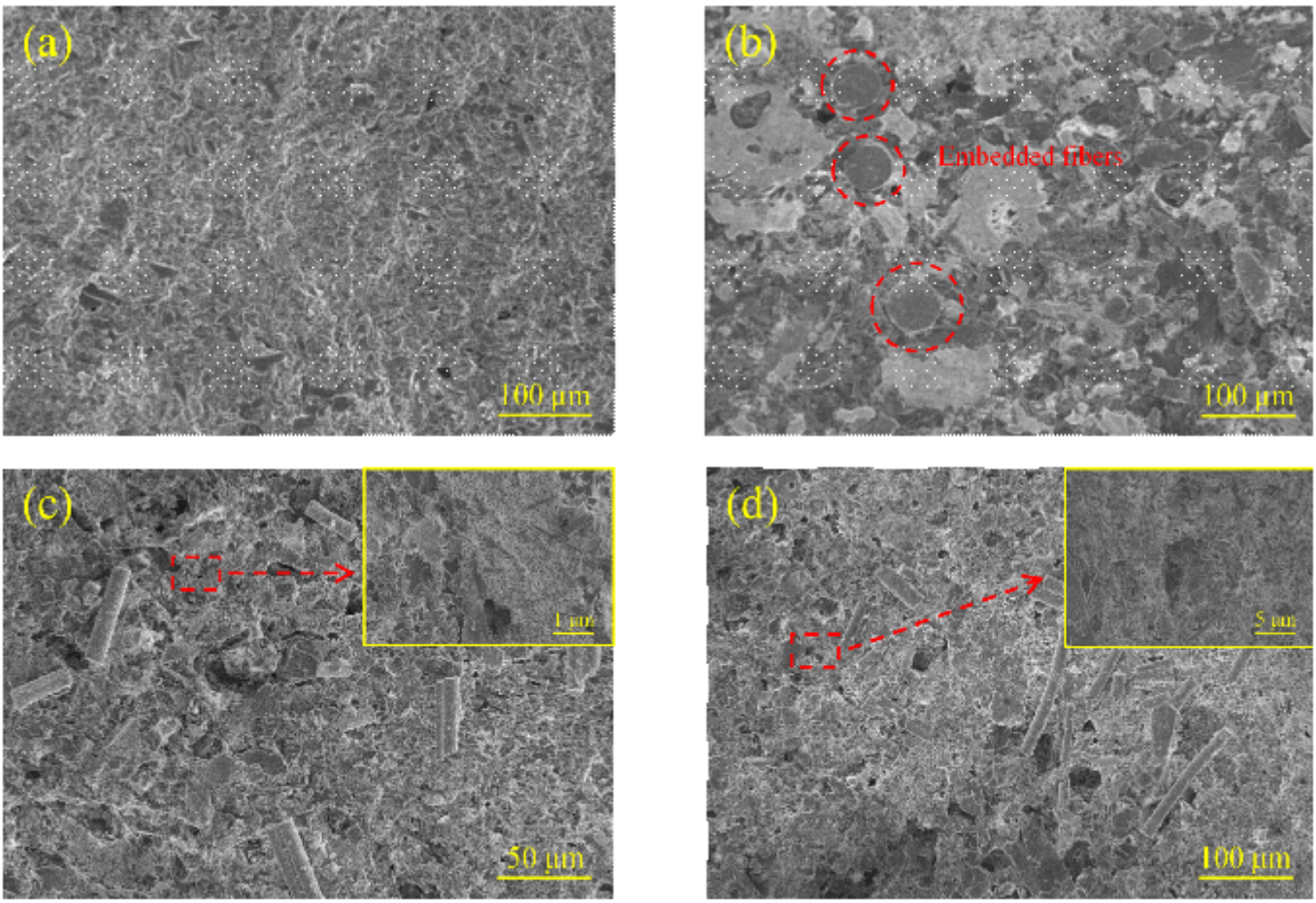

Figure 5

The cross-section SEM images of the as-prepared samples with different fiber contents; (a) blank sample; (b) 3 wt% fiber contents; (c) 5 wt% fiber contents; (d) 7 wt% fiber contents.

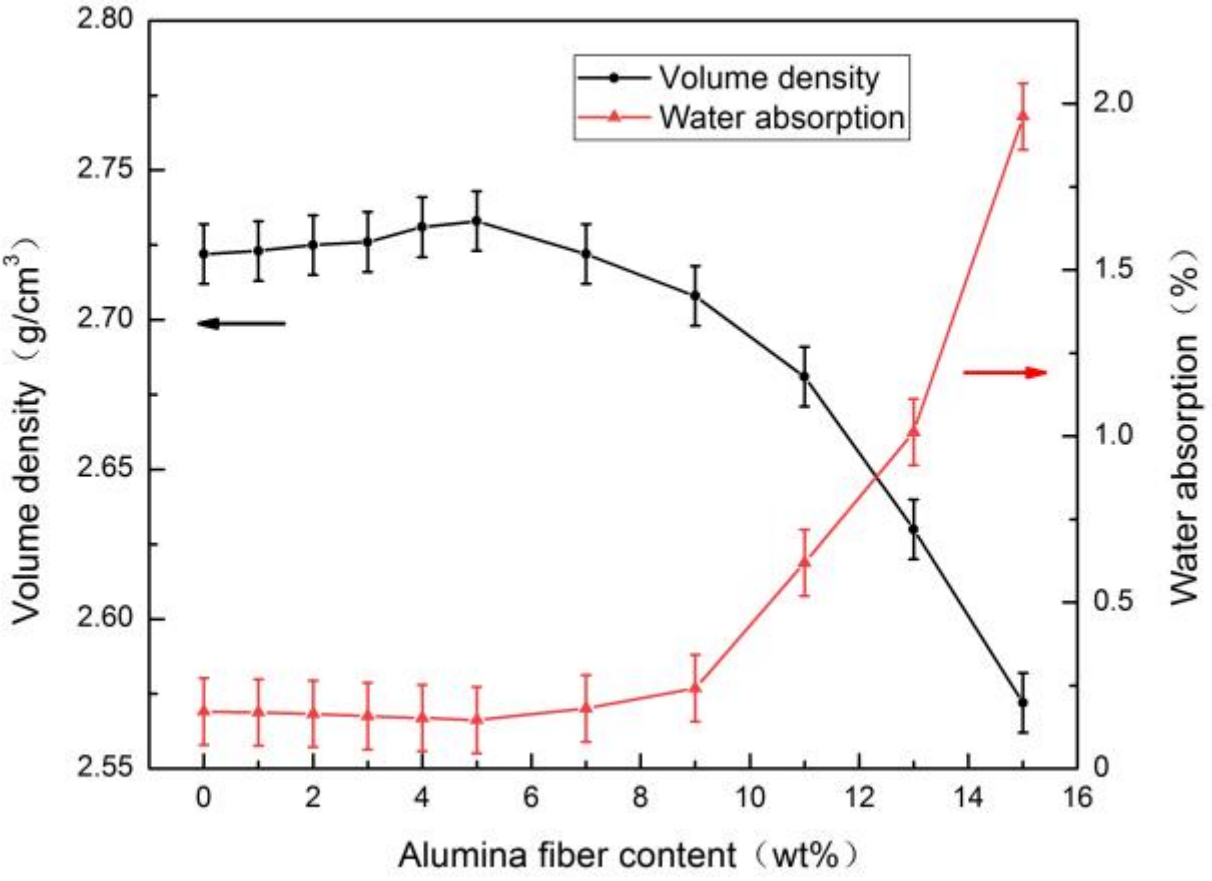

Figure 6

The volume density and water absorption of the thin architectural ceramic plate with different alumina fiber contents.

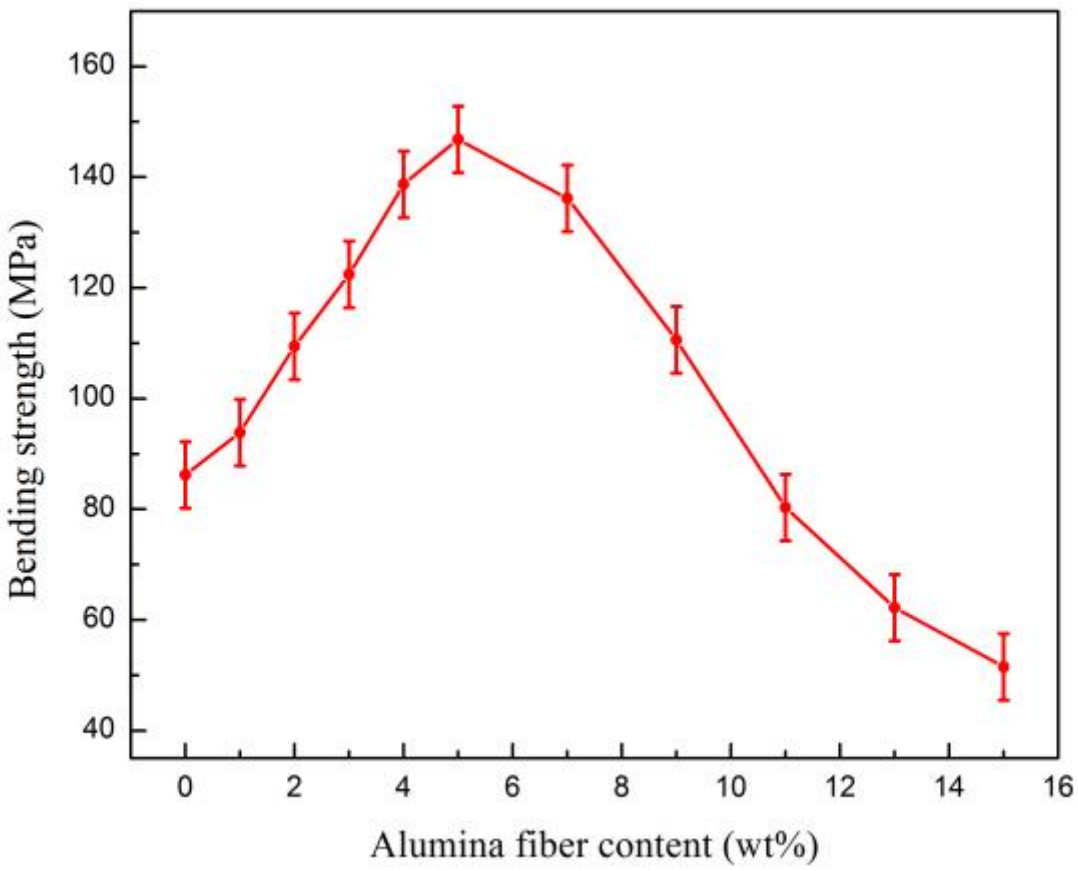

Figure 7

The bending strength of the thin architectural ceramic plate with different alumina fiber contents.

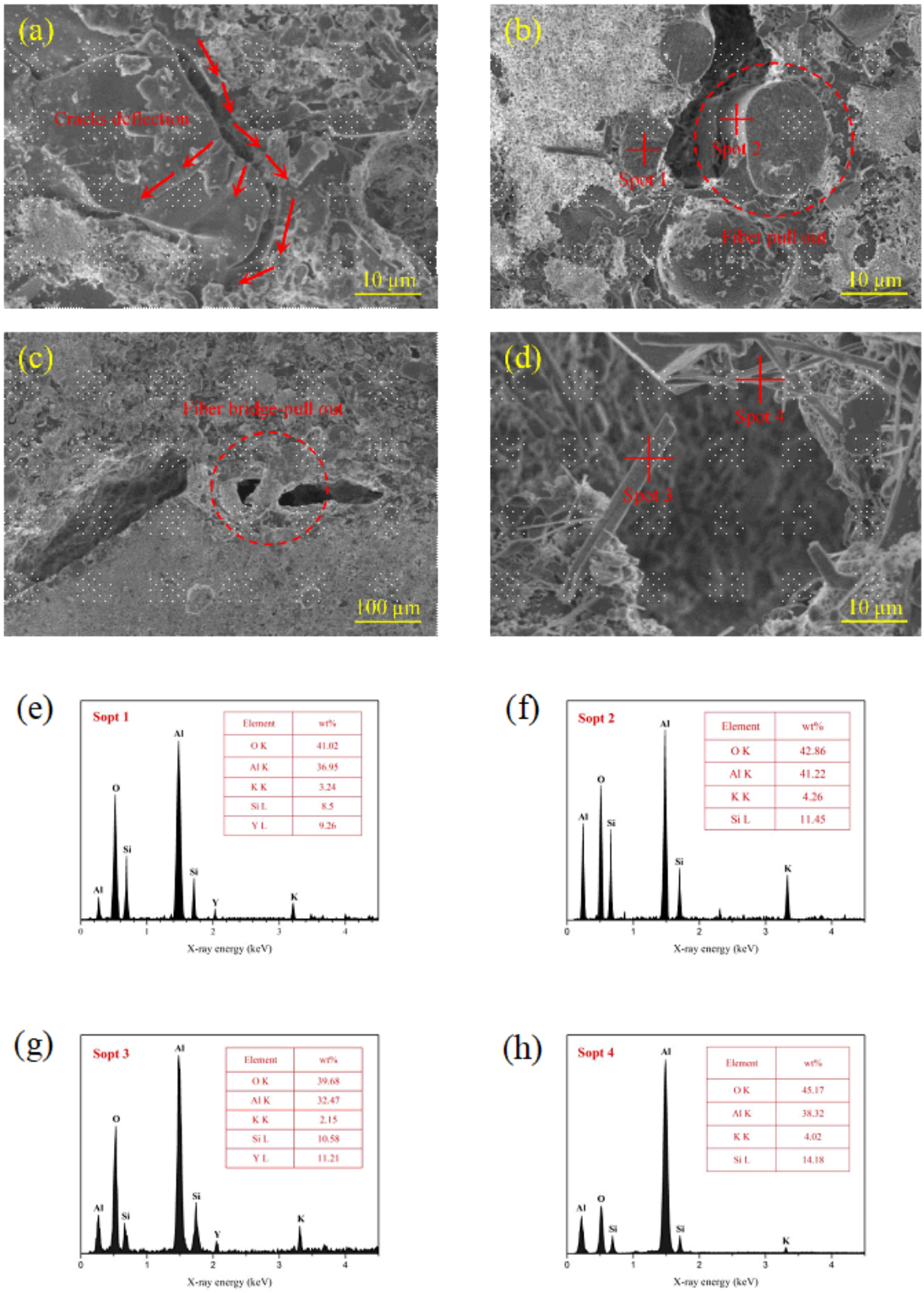

Figure 8

The cross-section SEM images of the as-prepared samples with 5 wt% alumina fibers contents; (a) micro-cracks deflection and particles diffusion enhancements; (b, c and d) fiber bridge-pull out from matrix; (e, f) the EDS analysis corresponding to the spot 1 and spot 2 in (b); (g, h) the EDS analysis corresponding to the spot 3 and spot 4 in (d).

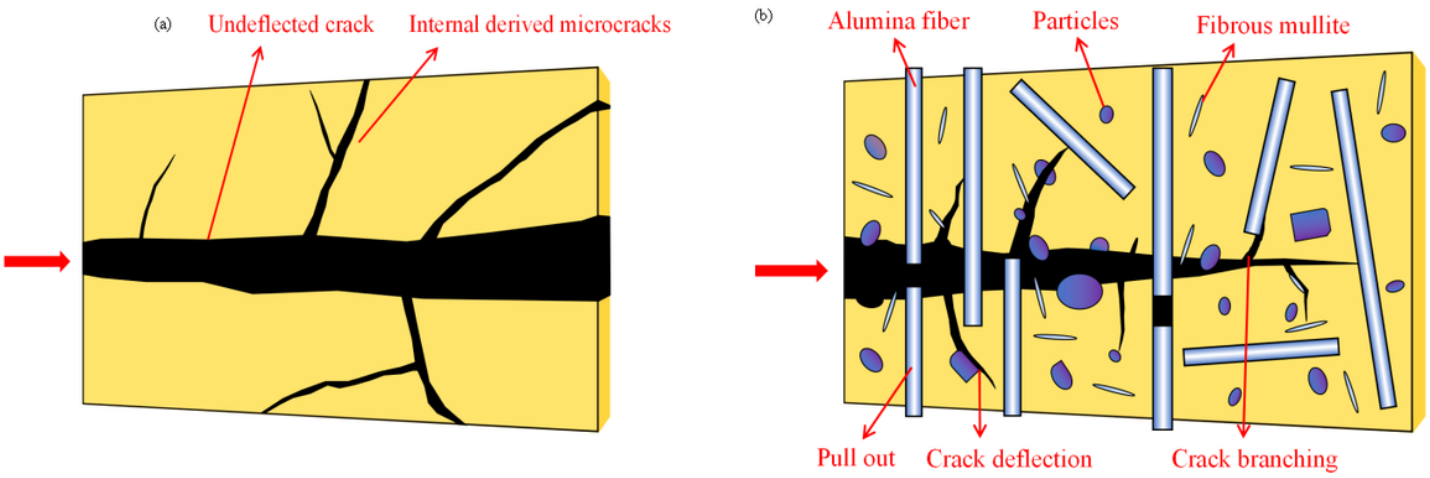

Figure 9

Diagrammatic sketch for the toughening mechanisms of the as-prepared thin architectural ceramic plate; (a) diffusion of micro-cracks in unreinforced matrix; (b) diffusion of micro-cracks in alumina fibers reinforced thin architectural ceramic plate.